Data Compression for Snapshot Mosaic Hyperspectral Image Sensors

George Tzagkarakis*, Wouter Charle† and Panagiotis Tsakalides*‡
*Institute of Computer Science (ICS) - Foundation for Research and Technology-Hellas (FORTH), Crete, Greece
†IMEC, Leuven, Belgium
‡Computer Science Department, University of Crete, Greece
Email: *gtzag@ics.forth.gr, wouter.charle@imec.be, tsakalid@ics.forth.gr*

***Abstract*—Recent achievements in hyperspectral imaging (HSI) demonstrated successfully a novel snapshot mosaic sensor architecture, enabling spectral imaging in a truly compact way. Integration of this new technology in handheld devices necessitates efficient compression of HSI data. However, due to the specific mosaic structure of the acquired images, traditional compression methods tailored to full-resolution HSI data cubes fail to exploit the special spatio-spectral interrelations among the pixels. This paper introduces an efficient and computationally tractable compression technique for mosaic HSI images. Specifically, an appropriate decorrelator is constructed for exploiting the spatio-spectral redundancies among the pixels, by modeling the filters arrangement on the mosaic HSI sensor as a multiple-input multiple-output antenna array. Doing so, the decorrelator depends only on the sensor and not on the data to be compressed. Comparison with state-of-the-art compression methods designed for HSI data cubes reveals that our approach achieves better reconstruction quality at lower bits-per-pixel rates.**

***Index Terms*—Hyperspectral data, snapshot mosaic hyperspectral sensor, image compression, spatio-spectral decorrelation.**

I. Introduction

Hyperspectral imaging (HSI), or imaging spectroscopy, combines the power of digital imaging and spectroscopy. For each pixel in an image, a hyperspectral camera acquires the light intensity (radiance) for a large number, typically a few tens to several hundreds, of contiguous spectral bands. Thus every pixel in the image contains a continuous spectrum (in radiance or reflectance), which can be used to characterize the objects in the scene with great precision and detail.

Recent technological advances in sensor design and processing speed have enabled a wide range of HSI applications in spaceborne remote sensing [1], industrial quality control [2], medicine [3], and biophysics [4]. Due to the rich information content of HSI measurements, there is a well-founded need for designing efficient compression algorithms in order to reduce the vast amount of data without degrading their quality.

Compression of HSI data is a challenging task, especially due to the huge amount of information, and the differences between the spatial and spectral correlation properties among the pixels. This challenge becomes even bigger with the latest achievements in the design of highly compact, low-cost, *snapshot mosaic* (SSM) imaging sensors, which pave the way for even more HSI applications by exploiting the advantages of snapshot acquisition. Due to the specific mosaic structure of SSM sensors, existing compression methods, which better adapt to full-resolution HSI data cubes, may fail to handle the reduced spatio-spectral pixel correlations of SSM HSI images.

In this paper, a computationally tractable method is introduced for efficient lossless/lossy compression of mosaic HSI images. Specifically, motivated by the spatio-spectral properties of multiple-input multiple-output (MIMO) antenna arrays, an appropriate spatio-spectral decorrelator is designed, which adapts to the specific arrangement of the filters on the mosaic sensor, thus it is computed only once for a given SSM sensor. Then, we employ a hybrid approach by first compressing across the spectral dimension, followed by a two-dimensional spatial compression of the transformed spectral bands. The experimental evaluation reveals for a given bits-per-pixel budget, our proposed method exhibits a better reconstruction performance when compared against state-of-the-art methods designed for full HSI data cube compression.

The rest of the paper is organized as follows: Section II describes the major technical features of a novel SSM image sensor designed by IMEC. Section III analyzes our proposed method for efficient, yet computationally effective, compression of mosaic HSI data. In Section IV, the performance of our method is evaluated in terms of the image reconstruction quality as a function of the achieved compression ratio (expressed in bits-per-pixel), and it is compared against state-of-the-art methods tailored to full-resolution HSI data cubes. Finally, Section V summarizes the main outcomes of this study and gives directions for further improvements.

II. IMEC's SSM Hyperspectral Image Sensor

When acquiring a three-dimensional (3D) hyperspectral data cube, there are four basic technologies, each with its own advantages and limitations. These technologies include: 1) *Spatial Scanning*: sensor output is either a two-dimensional (2D) full slit spectrum (push-broom scanner) or a one-dimensional (1D) full point-like spectrum (whisk-broom scanner). Platform movement or scanning, using complex mechanical parts, is required to capture a scene; 2) *Spectral Scanning*: sensor output represents a 2D monochromatic spatial map of the scene. Spectral smearing can occur if there is movement within the scene; 3) *Spatio-spectral Scanning*: sensor output represents a 2D wavelength-coded (staircase-like) spatial map of the scene. Scanning is required to capture the spectral content of a scene; 4) *Non-scanning (Snapshot HSI)*: a single 2D sensor

978-0-9928-6265-7/16/$31.00 ©2016 IEEE

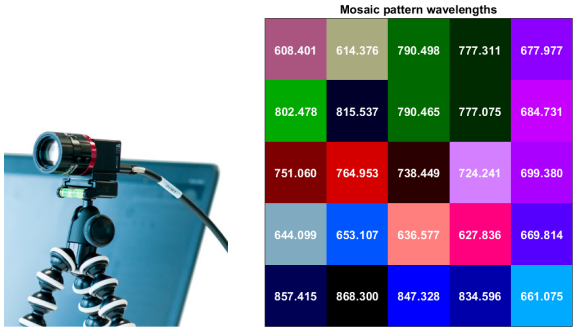

(a) SSM HSI imager (b) Filters arrangement

Fig. 1: SSM HSI imager used in our experimental setup, along with the filters arrangement on the 5×5 mosaic pattern.

output contains the full spatial and spectral information of a scene. Snapshot acquisition enables higher light throughput and shorter acquisition times. However, the extensive use of snapshot hyperspectral imagers has been hindered mainly because of the high manufacturing cost.

Fortunately, recent advances in the design of snapshot imaging sensors alleviate the limitations of previous sensor architectures. In particular, IMEC[1] has launched a new generation of SSM imagers [5], whose filter structures are processed on commercially available CMOS sensor wafers, enabling extremely compact, low-cost and mass-producible HSI devices. The newly developed mosaic sensors have one spectral filter deposited per pixel, arranged in mosaics of 4×4 (16 spectral bands) or 5×5 (25 spectral bands) covering an array of about 2 Megapixels. Their extended spectral range offers unique advantages compared to existing HSI linescan sensors for applications in which scanning is not practical.

Without loss of generality, in this study we rely on the 5×5 mosaic pattern. We should note that our proposed compression method, to be analyzed in Section III, is applicable to any $N_{f_V} \times N_{f_H}$ mosaic pattern (N_{f_V} and N_{f_H} denote the number of filters along the vertical and horizontal direction, respectively) and filter arrangement. Fig. 1a shows the camera, which is used to capture HSI images for our experimental evaluation. This camera is manufactured by Ximea[2] and is equipped with IMEC's 5×5 SSM sensor whose filters arrangement is shown in Fig. 1b. The sensor size (height x width) is 1088×2048 with an active area of 1080×2045 pixels. In the case of a 5×5 mosaic, this yields a spatial resolution of 216×409 pixels per band, which are stored using 10 bits-per-pixel. The spectral resolution is equal to 25 bands, which span the range $600 - 1000$ nm (Visible–NIR) with a spectral bandwidth (Full Width at Half Maximum (FWHM)) of 15 nm.

The specific mosaic structure of the SSM sensors poses certain constraints on the way of processing the acquired images. Specifically, it is important to account for the fact that each pixel captures a single wavelength, while the same wavelength appears again every 5 pixels in both the vertical and horizontal direction (or, for a generic mosaic pattern, every N_{f_V} and N_{f_H} pixels in the vertical and horizontal direction, respectively). As a result, neighboring pixels in the same spectral band do not correspond to adjacent pixels in the actual scene. It is exactly this unique spatio-spectral arrangement among the distinct pixels of a SSM sensor which makes the compression of mosaic HSI images a challenging task.

[1]http://www2.imec.be/be_en/home.html

[2]Ximea MQ022HG-IM-SM5X5-NIR sensor: http://goo.gl/nP4Bqg

III. Compression of SSM Hyperspectral Images

Existing scanning-based acquisition systems produce as an output a full-resolution HSI data cube. These data are typically characterized by strong correlations across their spectral bands, which are exploited by applying a 1D spectral decorrelating transformation prior to spatial coding. The state-of-the-art for compressing HSI data cubes includes techniques which are based on predictive compression [6], [7], vector quantization [8], [9], and transform coding (*e.g.,* by applying a 3D wavelet transform on the full data cube [10], or a combination of a 1D spectral decorrelator, such as the Karhunen-Loève transform (KLT) [11] or principal components analysis (PCA) [12], followed by JPEG2000).

Although the above methods exploit efficiently the spatio-spectral redundancies, they may be proven inefficient in the mosaic case. Furthermore, techniques that utilize KLT or PCA, which present a high spectral decorrelation performance in the full-resolution case, require an update of the associated transform matrices based on the input data, increasing significantly the overall computational burden.

In the following, we introduce a compression method for SSM images, which adapts to the specific mosaic structure of the sensor. The proposed method is motivated by the spatio-spectral properties of a multiple-input multiple-output (MIMO) antenna array, which is seen as an analogue to a mosaic pattern. Doing so, we overcome the limitations of previous methods when compressing mosaic HSI images, by adapting to the structure of the mosaic sensor, which is fixed, rather than to the acquired data. We also note that in the following, we focus on the design of the compression module, while the standard rate allocator and entropy coder of JPEG2000 are employed for the encoding part.

A. MIMO Antenna Arrays Analogue to SSM Imagers

The motivation for the design of our proposed compression method for mosaic images emerges from the observation that the mosaic pattern of a SSM sensor resembles a MIMO antenna array. Indeed, each filter of the mosaic pattern can be considered as an antenna on the planar array, with known filter response. The benefit of considering the SSM sensor as an antenna array is that we are capable of exploiting the well-known spatio-spectral correlation properties of MIMO antenna arrays, which depend on the arrangement and configuration of the antennas on the plane, or, equivalently, of the filters on the mosaic pattern of our SSM sensor. Doing so, we are able not only to exploit redundancies across the spectral bands, but also to account for the spatial effects of the mosaic structure.

B. Spatio-Spectral Decorrelation for SSM Sensors

Concerning the inter-filter spatial correlation, a single coefficient model was introduced in [13]. For simplicity, we consider a regular grid of equidistant filters both horizontally and vertically, at distance d. Let $\rho_s = \rho(d)$ denote the correlation coefficient between two adjacent filters, and N_f be the total number of filters (*e.g.,* $N_f = 25$ for the 5×5 mosaic pattern). Then, the *spatial correlation matrix*, $\mathbf{R}_S$, of the antenna array has the following Toeplitz structure

$$\mathbf{R}_S = \begin{bmatrix} 1 & \rho_s & \rho_s^4 & \cdots & \rho_s^{(N_f-1)^2} \\ \rho_s & 1 & \rho_s & \cdots & \rho_s^{(N_f-2)^2} \\ \vdots & \vdots & \vdots & \ddots & \vdots \\ \rho_s^{(N_f-1)^2} & \rho_s^{(N_f-2)^2} & \rho_s^{(N_f-3)^2} & \cdots & 1 \end{bmatrix} \tag{1}$$

To account for the specific spatial arrangement of the filters on the mosaic pattern, first, an order is assigned to each filter according to its position in the sorted wavelenghts vector (*e.g.,* the bottom right filter of the 5×5 pattern in Fig. 1b corresponds to the 7th smallest wavelength). Fig. 2a shows this spatial ordering of the filters according to an increasing wavelength. Then, the normalized (Euclidean) distance is computed for each pair of filters f_i, f_j, that is, $d_{i,j} = d(f_i, f_j)$ for $i, j = 1, \ldots, N_f$ (*e.g.,* $d(f_2, f_{21}) = 1$, $d(f_{21}, f_3) = 2\sqrt{2}$). By combining this spatial ordering with (1), we get the following generalization for the spatial correlation matrix of a SSM sensor

$$\mathbf{R}_S^{\text{SSM}} = \begin{bmatrix} 1 & \rho_s^{d_{1,2}} & \rho_s^{d_{1,3}} & \cdots & \rho_s^{d_{1,N_f}} \\ \rho_s^{d_{2,1}} & 1 & \rho_s^{d_{2,3}} & \cdots & \rho_s^{d_{2,N_f}} \\ \vdots & \vdots & \vdots & \ddots & \vdots \\ \rho_s^{d_{N_f,1}} & \rho_s^{d_{N_f,2}} & \rho_s^{d_{N_f,3}} & \cdots & 1 \end{bmatrix}. \tag{2}$$

The choice of ρ_s may affect the accuracy of $\mathbf{R}_S^{\text{SSM}}$. Although estimating precisely the value of ρ_s for our mosaic pattern is still an open issue, however, by varying ρ_s in $[0.9, 1)$ typically suffices for achieving a high compression performance. A more thorough study for the optimal selection of ρ_s is currently under way.

Similarly, the *spectral correlation matrix*, $\mathbf{R}_F$, of the antenna array is given by [14]. More specifically, let ρ_f denote the correlation coefficient between two adjacent filter elements, where the adjacency depends on the spectral resolution (1 nm for our SSM sensor), and f_i be the center frequency of the i-th filter, with the filters being sorted in ascending wavelength as in the spatial correlation case. Then, the spectral correlation matrix is modeled as follows,

$$\mathbf{R}_F = \frac{\sigma_f^2}{N_f} \begin{bmatrix} 1 & \rho_f & \rho_f^2 & \cdots & \rho_f^{N_f-1} \\ \rho_f & 1 & \rho_f & \cdots & \rho_f^{N_f-2} \\ \vdots & \vdots & \vdots & \ddots & \vdots \\ \rho_f^{N_f-1} & \rho_f^{N_f-2} & \rho_f^{N_f-3} & \cdots & 1 \end{bmatrix}, \tag{3}$$

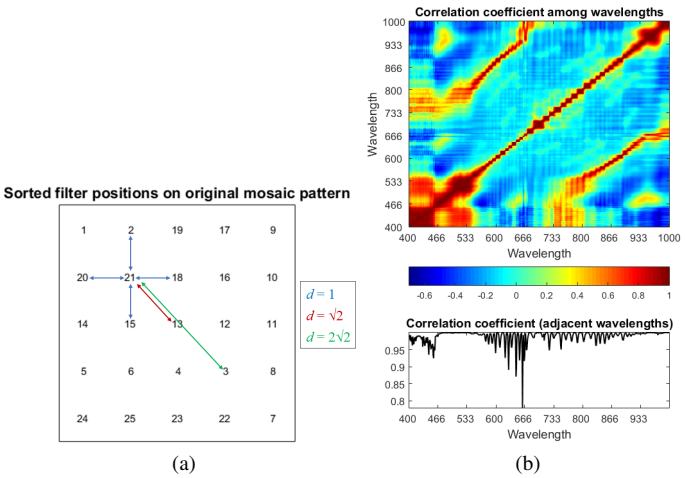

(a) (b)

Fig. 2: a) Sorted filter positions on original mosaic pattern according to increasing wavelength; b) Correlation coefficients among the filter responses of our 5×5 mosaic pattern. Bottom curve shows the correlation coefficients for 1 nm-adjacency.

where σ_f^2 represents the energy of the filter response. In the above formulation it is assumed that the center frequencies of the filters are normalized, that is, $f_i = i$. However, this assumption can be generalized by considering directly the real center frequencies of the mosaic pattern's filters. Then, by defining $f_{i,j} = |f_i - f_j|$ as the absolute difference between the center frequencies, we get the following expression for the spectral correlation matrix of a SSM sensor,

$$\mathbf{R}_F^{\text{SSM}} = \frac{\sigma_f^2}{N_f} \begin{bmatrix} 1 & \rho_f^{f_{1,2}} & \rho_f^{f_{1,3}} & \cdots & \rho_f^{f_{1,N_f}} \\ \rho_f^{f_{2,1}} & 1 & \rho_f^{f_{2,3}} & \cdots & \rho_f^{f_{2,N_f}} \\ \vdots & \vdots & \vdots & \ddots & \vdots \\ \rho_f^{f_{N_f,1}} & \rho_f^{f_{N_f,2}} & \rho_f^{f_{N_f,3}} & \cdots & 1 \end{bmatrix}. \tag{4}$$

The precise computation of σ_f^2 for our sensor is currently under study. However, since the scalar multiple of a matrix does not affect its eigenvectors, for simplicity we ignore the factor $\frac{\sigma_f^2}{N_f}$. The coefficient ρ_f is computed directly by averaging all pairwise correlation coefficients among the responses of the filters which are 1 nm-adjacent. Fig. 2b shows the pairwise correlation coefficients between all the filter responses, while the bottom curve corresponds to the correlations for 1 nm-adjacent wavelengths.

Having constructed the two correlation matrices, $\mathbf{R}_S^{\text{SSM}}$ and $\mathbf{R}_F^{\text{SSM}}$, for the SSM sensor, then, motivated by [15], the *joint spatio-spectral* correlation matrix $\mathbf{R}_{SF}^{\text{SSM}}$ is obtained as the Schur-Hadamard product

$$\mathbf{R}_{SF}^{\text{SSM}} = \mathbf{R}_S^{\text{SSM}} \odot \mathbf{R}_F^{\text{SSM}}, \tag{5}$$

where $\odot$ denotes the element-wise matrix multiplication.

Let $\mathbf{X} \in \mathbb{N}^{N_V \times N_H}$ denote a mosaic HSI image, where $N_V \times N_H$ is the active area of the sensor, which is tiled with a mosaic pattern of size $N_{f_V} \times N_{f_H}$ yielding $N_f = N_{f_V} \cdot N_{f_H}$

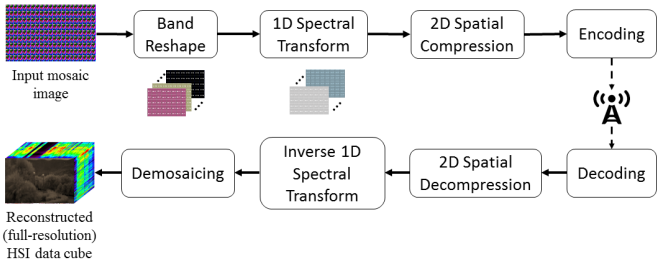

Fig. 3: Proposed compression pipeline for SSM HSI images.

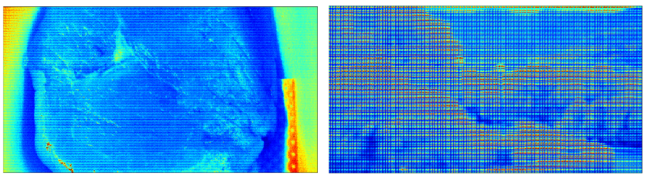

(a) Meat (b) Outdoor

Fig. 4: SSM HSI images, captured with a Ximea HSI imager equipped with IMEC's mosaic filters, used in our experimental evaluation.

spectral bands of size $N_{b_V} \times N_{b_H}$. Let also $\mathbf{b}^n$ denote the n-th band ($n = 1, \ldots, N_f$), $b^n_{i,j}$ be the pixel located in row i ($i = 1, \ldots, N_{b_V}$) and column j ($j = 1, \ldots, N_{b_H}$) of the n-th band, and $\mathbf{b}_{i,j} = [b^1_{i,j}, b^2_{i,j}, \ldots, b^{N_f}_{i,j}]^T$ denote the spectral vector for the (i,j)-th pixel. In our case, $N_V = 1080$, $N_H = 2045$, and $N_{f_V} = N_{f_H} = 5$ resulting in 25 spectral bands of size 216×409 pixels per band.

Following a PCA-based compression philosophy, first we decorrelate the spectral vectors, $\mathbf{b}_{i,j}$, by projecting onto an appropriate subspace. To this end, we compute the matrix $\mathbf{E} \in \mathbb{R}^{N_f \times N_f}$, whose columns are the eigenvectors of $\mathbf{R}^{\text{SSM}}_{SF}$. Then, each spectral vector $\mathbf{b}_{i,j}$ is projected onto the columns of $\mathbf{E}$ giving a vector of transformed spectral coefficients,

$$\mathbf{c}_{i,j} = \mathbf{E}^T \mathbf{b}_{i,j} \ . \tag{6}$$

Notice that, in general, $\mathbf{c}_{i,j} \in \mathbb{R}^M$ with $M \leqslant N_f$, where a lower-dimensional vector, $\mathbf{c}_{i,j} = \mathbf{E}^T_M \mathbf{b}_{i,j}$, is obtained by projecting on a subset of M eigenvectors, $\mathbf{E}_M$, corresponding to the M largest eigenvalues of $\mathbf{E}$.

Finally, each one of the 2D transformed bands, $\mathbf{c}^m$ ($m = 1, \ldots, M$) is compressed independently by means of a conventional 2D spatial compression method, such as JPEG2000. We emphasize again that in this work we focus on the compression module, while for the encoding part we employ the standard rate allocation mechanism and entropy coder of JPEG2000. Furthermore, although demosaicing is a critical component that affects the overall system performance, however, in the subsequent experimental evaluation we measure the similarity between the original and the reconstructed spectral bands, $\mathbf{b}^n$ and $\hat{\mathbf{b}}^n$ ($n = 1, \ldots, N_f$), respectively, whilst leaving the effect of demosaicing as a separate thorough study. Notice also that, due to the structure of the original mosaic image, the full-resolution spectral bands are not available to be used as a benchmark. Our proposed approach for compressing mosaic HSI images is summarized in Fig. 3.

IV. Experimental Evaluation

In this section, the performance of our proposed compression method is evaluated and compared against state-of-the-art methods designed for full-resolution HSI data cubes. Our data set consists of two distinct mosaic HSI images, shown in Fig. 4, which are captured by Ximea's HSI camera (ref. Fig. 1a) equipped with IMEC's 5×5 mosaic sensor. Our proposed approach (Fix1D-2D) is compared against three alternative methods, namely, 1) the naive method (JPEG2K-Full2D), which applies JPEG2000 compression to the original 2D mosaic image; 2) a transform coding method (JPEG2K-Band2D), which first reshapes the original mosaic image into 25 spectral bands and then compresses the 3D data cube by applying a hybrid 1D(spectral)-2D(spatial) discrete wavelet transform (DWT); 3) a hybrid 1D-2D compression method (PCA-2D) similar to 2), which first decorrelates the spectral vectors using PCA and then applies JPEG2000 for 2D spatial compression. In this evaluation, both our method and the PCA-based one employ all of their 25 eigenvectors, however, scalable coding is supported by varying the number, M, of retained eigenvectors. In all cases, the lossless/lossy operation of the compression module is controlled by JPEG2000, whose parameters are kept fixed for all the above methods.

The reconstruction quality of the decompressed HSI data, $\hat{\mathbf{X}}$, is measured in terms of the average peak signal-to-noise ratio (PSNR) and average structural similarity index (SSIM), where the average is taken over the $N_f = 25$ spectral bands:

$$\text{PSNR}\left(\mathbf{X}, \hat{\mathbf{X}}\right) = 10 \cdot \log_{10}\left(\frac{\left(\max(\mathbf{X})\right)^2}{\frac{\sum_{n,i,j}\left(b^n_{i,j} - \hat{b}^n_{i,j}\right)^2}{N_f N_{b_V} N_{b_H}}}\right), \tag{7}$$

$$\text{SSIM}\left(\mathbf{X}, \hat{\mathbf{X}}\right) = \frac{1}{N_f}\sum_n \frac{\left(2\mu_{\mathbf{b}^n}\mu_{\hat{\mathbf{b}}^n} + c_1\right)\left(2\sigma_{\mathbf{b}^n\hat{\mathbf{b}}^n} + c_2\right)}{\left(\mu^2_{\mathbf{b}^n} + \mu^2_{\hat{\mathbf{b}}^n} + c_1\right)\left(\sigma^2_{\mathbf{b}^n} + \sigma^2_{\hat{\mathbf{b}}^n} + c_2\right)}, \tag{8}$$

where $\mu_\cdot$, $\sigma_\cdot$, and $\sigma_{\cdot,\cdot}$ denote the mean, standard deviation, and correlation coefficient of the spectral bands, respectively, while c_1 and c_2 are parameters for numerical stabilization.

Fig. 5 shows the achieved PSNR and SSIM values, as a function of the required bits-per-pixel (bpp), for the two mosaic images and the four compression methods. As expected, compressing directly the full mosaic image (JPEG2K-Full2D) yields the worst performance for both test images, due to the lack of strong spatio-spectral redundancies in the mosaic image. On the other hand, our proposed method (Fix1D-2D) exhibits a better reconstruction quality for a given bpp value. This is more prominent in the case of the "Meat" image and for the corresponding SSIM values. For the "Outdoor" image we observe that both the PSNR and SSIM values for our proposed method and the other two 1D-2D methods are very close to each other. However, our Fix1D-2D achieves again

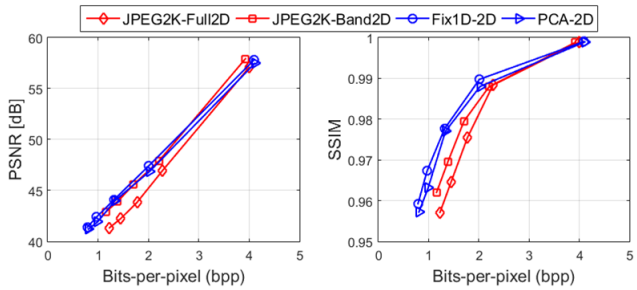

(a) Meat

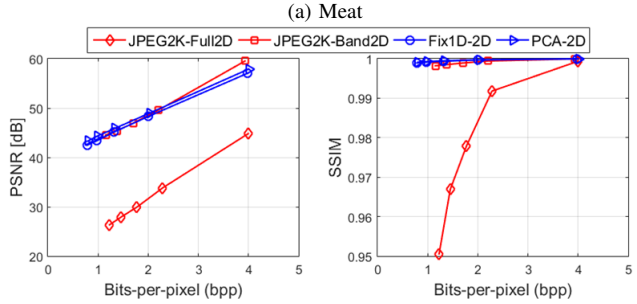

(b) Outdoor

Fig. 5: PSNR and SSIM as a function of the required bits-per-pixel for the SSM HSI images a) "Meat" and b) "Outdoor".

a comparable or even better quality by allocating fewer bpp, especially when operating in the low bpp regime.

A significant remark is that our method achieves a high performance, while being computationally very efficient. Indeed, in contrast to PCA-2D, whose spectral decorrelating matrix needs to be recalculated for every new input image, the decorrelating matrix of our method has to be computed only once for a given SSM sensor, and is then kept fixed for any input image. Furthermore, when compared against JPEG2K-Band2D, our proposed approach has a similar computational cost ($N_f^2 \approx N_f$ for our sensor), whilst it is better capable of exploiting the limited spectral correlations across the bands, by accounting for the specific spatio-spectral arrangement of the filters on the mosaic pattern. Table I gives a rough estimation of the computational burden of the three hybrid 1D-2D techniques.

TABLE I: Computational cost of the three hybrid 1D-2D compression techniques ($\mathcal{C}_{\text{JPEG2K}}$ denotes the complexity of JPEG2000 for compressing a $N_{b_V} \times N_{b_H}$ image).

Fix1D-2D	$\underbrace{\mathcal{O}(N_f^2 N_{b_V} N_{b_H})}_{\text{Spectral compression}} + \underbrace{N_f \cdot \mathcal{C}_{\text{JPEG2K}}}_{\text{Spatial compression}}$
JPEG2K-Band2D	$\underbrace{\mathcal{O}(N_f N_{b_V} N_{b_H})}_{\text{Spectral compression}} + \underbrace{N_f \cdot \mathcal{C}_{\text{JPEG2K}}}_{\text{Spatial compression}}$
PCA-2D	$\underbrace{\left(N_f^2 N_{b_V} N_{b_H} + \mathcal{O}(N_f^3)\right)}_{\text{PCA}} + \underbrace{\mathcal{O}(N_f^2 N_{b_V} N_{b_H})}_{\text{Spectral compression}} + \underbrace{N_f \cdot \mathcal{C}_{\text{JPEG2K}}}_{\text{Spatial compression}}$

V. Conclusions

In this paper, we introduced a method for compressing SSM HSI images. Motivated by the spatio-spectral properties of MIMO antenna arrays, a fixed spatio-spectral decorrelating matrix was constructed, which adapts to the specific mosaic filter structure of a SSM HSI sensor. Our proposed technique achieves comparable or even improved reconstruction performance, while operating at a lower bpp rate, when compared against the naive 2D compression approach, as well as against two state-of-the-art hybrid 1D-2D transform coding methods.

The incorporation of an efficient demosaicing algorithm, adapted to the specific mosaic pattern, along with a thorough study of its effect on the overall system performance, will be carried out in order to complete the pipeline of our HSI compression system, as shown in Fig. 3. Furthermore, the compression gain of a mosaic pattern, which can be computed from the spatio-spectral correlation matrix $\mathbf{R}_{SF}^{\text{SSM}}$, will be studied as a function of the filters arrangement, thus supporting the optimal arrangement of the filters on the sensor wafer in order to maximize the compression gain.

Acknowledgment

This work was funded by the European Union's Horizon 2020 research and innovation programme PHySIS under grant agreement No 640174.

References

[1] The Hyperspectral Precursor and Application Mission (PRISMA), Online: https://goo.gl/67sf1r.
[2] D.-W. Sun, "Hyperspectral Imaging for Food Quality Analysis and Control," Academic Press, 2010.
[3] G. Lu and B. Fei, "Medical hyperspectral imaging: a review," *J. of Biomed. Opt.*, **19**(1), 010901, Jan. 2014.
[4] J. W. Uhr *et al.*, "Molecular profiling of individual tumor cells by hyperspectral microscopic imaging," *Transl. Res.*, **159**(5), pp. 366–375, May 2012.
[5] IMEC Hyperspectral Mosaic Snapshot Imager brochure, Online: http://goo.gl/dgtfj8.
[6] B. Aiazzi, S. Baronti, and L. Alparone, "Lossless compression of hyperspectral images using multiband lookup tables," *IEEE Sig. Proc. Lett.*, **16**(6), pp. 481–484, 2009.
[7] D. Keymeulen *et al.*, "GPU lossless hyperspectral data compression system for space applications," *in Proc. IEEE Aerosp. Conf.*, Big Sky, MT, Mar. 2012.
[8] Y. Liu and W. Pearlman, "Multistage lattice vector quantization for hyperspectral image compression," *in Proc. Asilomar Conf. on Signals, Systems and Comp.*, Pacific Grove, CA, Nov. 2007.
[9] X. Li *et al.*, "Novel multivariate vector quantization for effective compression of hyperspectral imagery," *Opt. Comm.*, **332**, pp. 192–200, July 2014.
[10] E. Christophe, C. Mailhes, and P. Duhamel, "Hyperspectral image compression: Adapting SPIHT and EZW to anisotropic 3-D wavelet coding," *IEEE Trans. on Image Proc.*, **17**(12), pp. 2334–2346, Dec. 2008.
[11] B. Penna, T. Tillo, E. Magli, and G. Olmo, "Transform coding techniques for lossy hyperspectral data compression," *IEEE Trans. on Geosc. & Remote Sens.*, **45**(5), pp. 1408–1421, May 2007.
[12] D. Qian, L. Nam, and J. Fowler, "An operational approach to PCA+JPEG2000 compression of hyperspectral imagery," *IEEE J. Sel. Top. in App. Earth Obs. & Remote Sens.*, **7**(6), pp. 2237–2245, 2014.
[13] A. van Zelst and J. Hammerschmidt, "A single coefficient spatial correlation model for multiple-input multiple-output (MIMO) radio channels," *in Proc. URSI XXVIIth General Assembly*, Aug. 2002.
[14] W. Pratt and C. Mancill, "Spectral estimation techniques for the spectral calibration of a color image scanner," *App. Opt.*, **15**(1), pp. 73–75, 1976.
[15] X. Hong *et al.*, "On space-frequency correlation of UWB MIMO channels," *IEEE Trans. on Vehic. Tech.*, **59**(9), Nov. 2010.